Remote Sensing of Environment 112 (2008) 2950–2962

Contents lists available at ScienceDirect

Remote Sensing of Environment

journal homepage: www.elsevier.com/locate/rse

Global characterization of biomass-burning patterns using satellite measurements of fire radiative energy

Charles Ichoku [a,d,*], Louis Giglio [b,d], Martin J. Wooster [c], Lorraine A. Remer [d]

[a] ESSIC, University of Maryland, College Park, MD 20742, USA
[b] Science Systems & Applications, Inc., Lanham, MD 20706, USA
[c] King's College London, Department of Geography, Strand, London WC2R 2LS, UK
[d] NASA Goddard Space Flight Center, Greenbelt, MD 20771, USA

ARTICLE INFO

Article history:
Received 13 September 2007
Received in revised form 8 February 2008
Accepted 9 February 2008

Keywords:
Biomass burning
Wildfire
Fire radiative power (FRP)
Fire radiative energy (FRE)
MODIS

ABSTRACT

Remote sensing is the most practical means of measuring energy release from large open-air biomass burning. Satellite measurement of fire radiative energy (FRE) release rate or power (FRP) enables distinction between fires of different strengths. Based on a 1-km resolution fire data acquired globally by the MODerate-resolution Imaging Spectro-radiometer (MODIS) sensor aboard the Terra and Aqua satellites from 2000 to 2006, instantaneous FRP values ranged between 0.02 MW and 1866 MW, with global daily means ranging between 20 and 40 MW. Regionally, at the Aqua-MODIS afternoon overpass, the mean FRP values for Alaska, Western US, Western Australia, Quebec and the rest of Canada are significantly higher than these global means, with Quebec having the overall highest value of 85 MW. Analysis of regional mean FRP per unit area of land (FRP flux) shows that at peak fire season in certain regions, fires can be responsible for up to 0.2 W/m^2 at peak time of day. Zambia has the highest regional monthly mean FRP flux of ~ 0.045 W/m^2 at peak time of day and season, while the Middle East has the lowest value of ~ 0.0005 W/m^2. A simple scheme based on FRP has been devised to classify fires into five categories, to facilitate fire rating by strength, similar to earthquakes and hurricanes. The scheme uses MODIS measurements of FRP at 1-km resolution as follows: category 1 (<100 MW), category 2 (100 to <500 MW), category 3 (500 to <1000 MW), category 4 (1000 to <1500 MW), category 5 (≥1500 MW). In most regions of the world, over 90% of fires fall into category 1, while only less than 1% fall into each of categories 3 to 5, although these proportions may differ significantly from day to day and by season. The frequency of occurrence of the larger fires is region specific, and could not be explained by ecosystem type alone. Time-series analysis of the proportions of higher category fires based on MODIS-measured FRP from 2002 to 2006 does not show any noticeable trend because of the short time period.

1. Introduction

Fires burn extensive areas in different vegetated landscapes across the globe, and constitute a major disturbance to land-based ecosystems, such as forests and savannas. For instance, the total global burned area has been estimated at 3.5 million km^2 in year 2000 alone (Tansey et al., 2004), and 2.97–3.74 million km^2/year in 2001–2004 (Giglio et al., 2006b). By voraciously consuming biomass, releasing intense heat energy, and emitting thick plumes of smoke into the atmosphere, such large-scale fires exert several adverse effects on life, property, the environment, weather, and climate both directly and indirectly.

Correct assessment of fire impacts requires accurate documentation of where and when the fires occur, their size and/or strength, the amount of biomass burned, and the quantity of particulate and gaseous matter emitted in the smoke. Unlike most other physical objects and phenomena, because of the exothermic, aggressive, and erratic nature of large fires, their characteristics cannot be measured quantitatively in situ or even at close range. As such, alternative means of fire characterization includes judging its strength from measurements of the radiative component of its heat energy release, which can be sensed from a great distance.

Measures of Fire Radiative Energy (FRE) are currently being provided with specialized satellite-borne sensors, such as the MODerate-resolution Imaging Spectroradiometer (MODIS) aboard the Earth Observing System (EOS) Terra and Aqua polar-orbiting satellites (Kaufman et al., 1998) and the Spinning Enhanced Visible and Infrared Imager (SEVIRI) onboard the Meteosat-8 (formerly Meteosat Second Generation) geostationary satellite (Roberts et al., 2005). However, since every observation by these sensors lasts only an instant, what they actually measure is the rate of release of FRE per unit time (R_{fre}) or Fire Radiative Power (FRP) in MW (Kaufman et al., 1998; Wooster et al., 2003; Giglio et al., 2006a). A number of recent studies using small experimental fires have demonstrated that the total FRE

* Corresponding author. NASA Goddard Space Flight Center, Code 613.2, Greenbelt, MD 20771, USA.
E-mail address: Charles.Ichoku@nasa.gov (C. Ichoku).

0034-4257/$ – see front matter © 2008 Elsevier Inc. All rights reserved.
doi:10.1016/j.rse.2008.02.009

released over the lifetime of a fire has a simple linear relationship with the total amount of fuel biomass consumed (Wooster, 2002; Wooster et al., 2005). That relationship has been utilized to estimate the total biomass consumed over periods ranging from a few days to several months, using FRP measurements from the SEVIRI sensor, which acquires data every 15 min over Africa and Europe (Roberts et al., 2005). In a different study, MODIS-derived FRP measures have been analyzed in combination with aerosol optical thickness (AOT) measurements from the same sensor to derive a simple linear relationship between FRP and the rate of emission of smoke particulate matter (PM or aerosol) in various regions of the world (Ichoku & Kaufman, 2005). These studies have been able to demonstrate the strategic importance of satellite-measured FRP, and where possible, its time integrated product (FRE), as an efficient, relatively direct and realistic means of achieving both improved estimates of burned biomass and smoke emissions from open air biomass-burning activities, regionally or globally. Such data can facilitate improved evaluation of the impact of such fires on atmospheric composition, ecosystem status, climate, weather, health and security.

The objective of this study is to examine the spatio-temporal pattern of global biomass burning over the last several years. Effort is geared toward making a significant contribution to the knowledge base for fire assessment, by analyzing multi-year satellite-derived fire detections and FRP observations acquired globally from the Terra and Aqua MODIS sensors, as a measure of fire prevalence and intensity. Such an analysis will enable a detailed characterization of the range of fire-related ecosystem disturbances and smoke emission sources, thereby providing some satellite-oriented baselines that will ultimately allow the parameterization of these phenomena from satellite fire measurements to be improved in land-surface and atmospheric models. The overall aim is to contribute toward a clearer quantitative understanding of the total impact of fires on climate and vice versa than exists to date.

2. Satellite fire radiative power (FRP) data

The MODIS sensor is currently the only instrument that measures FRP globally on a daily basis, and provides all of the fire data used herein. It is a multi-spectral sensor with 36 spectral bands, ranging in wavelength from 0.4 to 14.2 μm (Salomonson et al., 1989), and fires are detected at 1-km spatial resolution (at nadir) using radiance measurements in the 4 μm and 11 μm channels. Measurements at several spectral bands are utilized for masking clouds, extremely bright surfaces, glint, and other potential sources of false alarms (Giglio et al., 2003). In the operational MODIS algorithm, only the 4-μm channel measurements are used to calculate FRP, based on the measured brightness temperatures of the fire pixel and its neighboring surface background (Kaufman et al., 1998). There are two 4-μm channels on

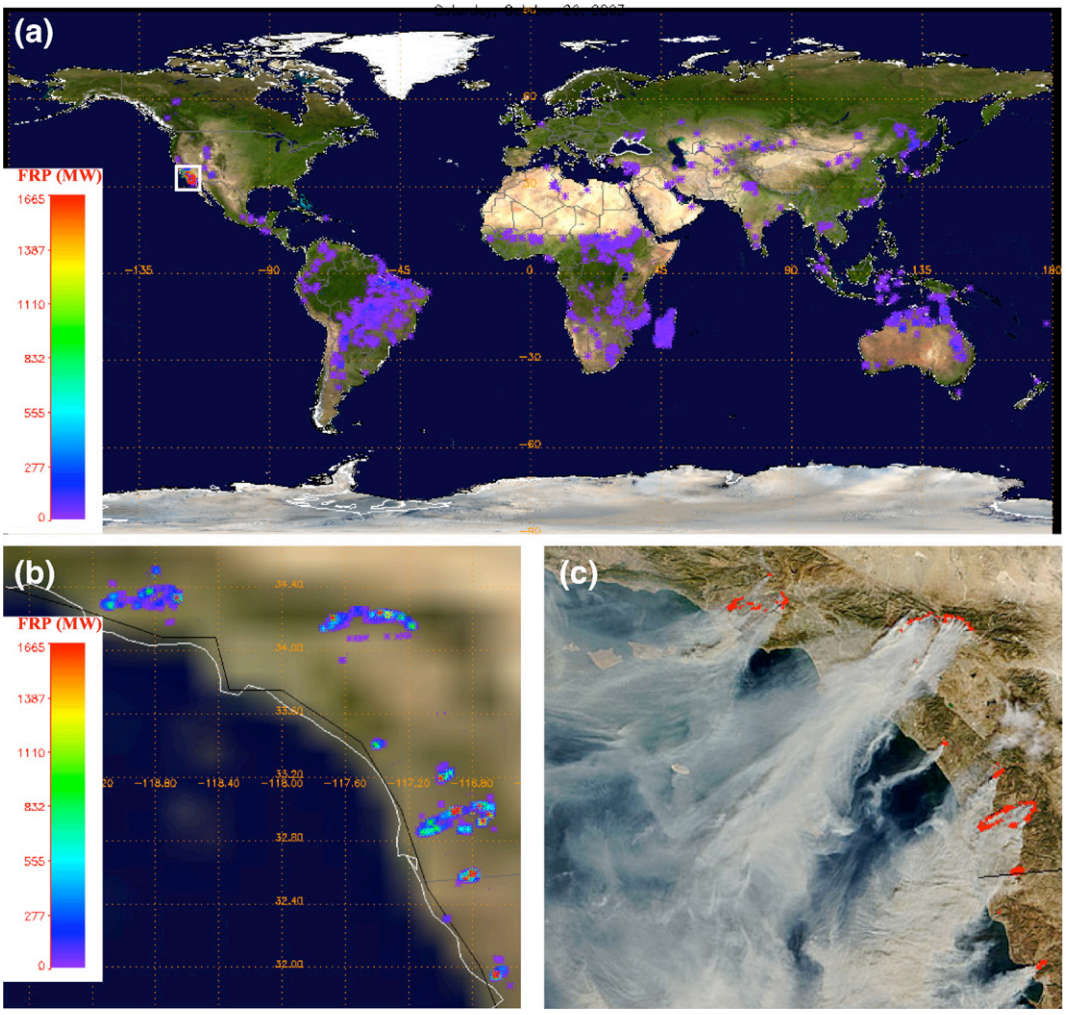

Fig. 1. Terra-MODIS daytime fire measurements on 26 October 2003, showing: (a) color-coded fire radiative power (FRP) values of fire pixels detected throughout the globe plotted over a MODIS-derived true-color image, with a white box delineating the most intense hotspot of that day, which occurred in California; (b) a close-up view of the FRP distribution of the California fires; (c) a true-color image of the same fire scene, with the fire pixels shown in red and the fire-emitted grayish white thick smoke plumes being advected over the adjoining Pacific Ocean.

each MODIS sensor, one of which is a 'low-gain' channel that can record pixel-integrated brightness temperatures of up to ~ 500 K, thereby allowing unsaturated measurements to be made over even very large/most intensely burning wildfires.

MODIS is a twin sensor flying on two NASA Earth Observing System (EOS) satellites: Terra (launched 19 December 1999) and Aqua (launched 4 May 2002). They are both polar orbiting, with Terra crossing the equator at approximately 10:30 AM and 10:30 PM local time, and Aqua at approximately 1:30 AM and 1:30 PM local time. Each MODIS sensor achieves near-global coverage once per day and once per night every 24 h, with higher latitude locations observed slightly more frequently because of increasingly large overlaps from successive satellite passes. Therefore, most fires detectable at a 1-km spatial resolution have the potential to have their FRP measured four times a day, except when covered by thick meteorological cloud. MODIS algorithms (including the fire algorithm) are updated periodically, leading to different versions, which are used to generate a series of Collections of the data products. The latest 'Collection 5' fire data were still under production at the time of writing, and so the penultimate Collection 4 data (Giglio et al., 2003) are used here, including all MODIS fire data products acquired from Terra (MOD14) and Aqua (MYD14) from the middle of 2002 to the end of 2006.

Globally, by examining all MODIS Collection 4 data (Terra and Aqua) acquired from the inception of usable data acquisition by each sensor (25-Feb-2000 for Terra and 25-June-2002 for Aqua) to the end of 2006, the overall minimum and maximum values of FRP per (1 x 1-km) pixel were found to be 0.021 MW and 1861.3 MW, respectively. Since there was only one value of 1861.3 MW (with a 4-μm brightness temperature of 506.6 K) and only very few cases of FRP values exceeding 1700 MW throughout the world in the time period considered, it can be said that measurement of FRP by MODIS is essentially unaffected by saturation. It is pertinent to mention that saturation is generally more apparent in sensor raw digital counts, which were not examined here. However, based on the distribution of the brightness temperature data examined, even if saturation exists, there can be only a very few cases, which are essentially negligible. This can be contrasted with older sensors, such as the Advanced Very High Resolution Radiometer (AVHRR) and the Along Track Scanning Radiometer (ATSR), whose fire detection channels (3.75 μm and 3.7 μm, respectively) saturated at around 322 K and 312 K, respectively (e.g. Giglio et al., 1999; Kelhä et al., 2003), thereby making them unsuitable for measuring FRP. Indeed, MODIS was the first, and currently only operating, spaceborne sensor in which FRP measurement was specifically taken into consideration during its design. It is not easy to validate satellite FRP measurements directly, but FRP data from MODIS have been compared with those from the Bi-spectral InfraRed Detection (BIRD) small satellite (Wooster et al., 2003) and SEVIRI (Roberts et al., 2005), and found to be highly correlated, with $r^2 = 0.99$ against BIRD and $r^2 = 0.83$ against SEVIRI. However, detailed comparison showed that SEVIRI (~ 3-km resolution) underestimates FRP by up to 40% with respect to MODIS (1-km resolution), which in turn underestimated FRP by up to 46% compared to BIRD (370-m resolution) in the relatively few cases examined. This sensor-to-sensor relative FRP underestimation is attributed to reduced sensitivity to smaller or cooler fires as spatial resolution decreases, while their mutual high correlations indicate that the general variation in FRP magnitude is indeed captured by the three sensors in a comparable manner.

Fig. 1a shows a MODIS-derived true-color global map of the earth, with color-coded FRP measurements from the daytime Terra-MODIS overpass on 26 October 2003 overlaid. The strongest fires on that day (enclosed by the white box) were found in the state of California in the United States, where the FRP values of certain pixels exceeded 1660 MW, while other parts of the world only had FRP values of the order of 300 MW or lower per pixel. A close-up view of this intensely emitting hot spot region (Fig. 1b) reveals further details of the FRP distribution, and a corresponding true-color image (Fig. 1c) shows the fire scene with prominent grayish-white thick smoke plumes being emitted into the atmosphere and the fire pixels shown in red.

MODIS global mean FRP values were calculated on a daily basis for the four Terra and Aqua local overpass times, and were found to range mostly between 20 and 40 MW, with occasional lower or higher values but almost never below 15 MW nor above 80 MW (Fig. 2a). There is no significant difference between the global mean FRP for the four overpass times. In contrast, there is a marked, almost two orders of magnitude, difference in the number of fire pixels (NFP or fire pixel counts) observed at the four MODIS overpass times (Fig. 2b), with the least number detected in the early morning hours (Aqua Night, around 1:30 AM local time), and the largest in the afternoon (Aqua Day, around 1:30 PM local time). Although vegetation fires have essentially similar general combustion and energy release characteristics, the specific characteristics of the biomass fuel (e.g. density, dryness) and weather conditions (e.g. wind speed, relative humidity) at a particular site significantly influences the fire size, rate of combustion, and thus the FRP measures. Therefore, different regions are likely to exhibit different spatio-temporal FRP patterns. Indeed, MODIS measurements of FRP have already been used to show that boreal fires in North America burn on average more intensely than those in Russia (Wooster & Zhang, 2004; Giglio et al., 2006a).

3. Methodology

3.1. Geobotanical considerations

To enable a detailed study of fire activity patterns in different parts of the world, both independently and comparatively, 36 regions in which fires generally occur have been identified on a MODIS-derived

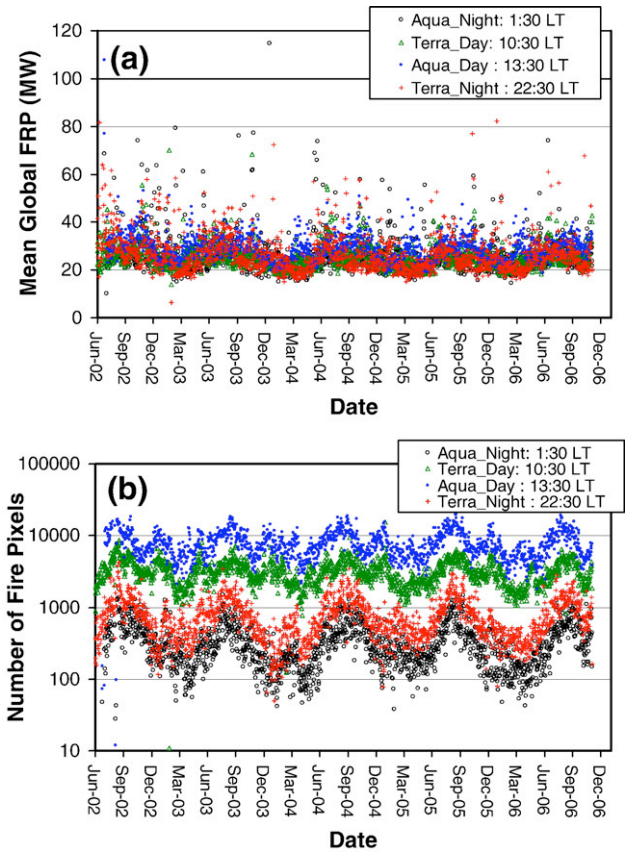

Fig. 2. Time series plots of MODIS daily global (a) mean fire radiative power (FRP) per pixel, and (b) total number of fire pixels (NFP or fire counts) without considering the effect of cloud cover.

ecosystem map of the world (Fig. 3a). Although it is impossible to restrict each region to only a single ecosystem type, effort has been made to ensure at least that each region can be associated with one major ecosystem type. The labeling of the boxed regions is only based on convenience, and does not conform to political boundaries.

The 36 'fire regions' are listed in Table 1, with their corresponding box numbers (from Fig. 3a), bounding box-corner coordinates, and abbreviated names to be used in the remainder of this paper. The fire regions have been clustered in six groups based on geographical proximity, while trying to the best extent possible to equalize the number of regions in each group in order to facilitate the analysis. The land surface area bounded by each of the boxes in Fig. 3a were calculated using a table of areas of quadrilaterals of 1-deg×1-deg on the earth's surface provided by Robinson & Sale (1969, Table D.3) and subtracting the areas labeled as water in the ecosystem map (Fig. 3a). The total area enclosed by the boxes and the corresponding land-only areas are listed in Table 1.

Proportions of seven broad ecosystem groupings in these fire regions are shown in Fig. 3b, which, in an effort to avoid excessive clutter, was derived by combining some of the 16 land-only land-cover classes (shown in Fig. 3a) that are typically collocated geographically or have the same characteristics in relation to fires, such as barren and

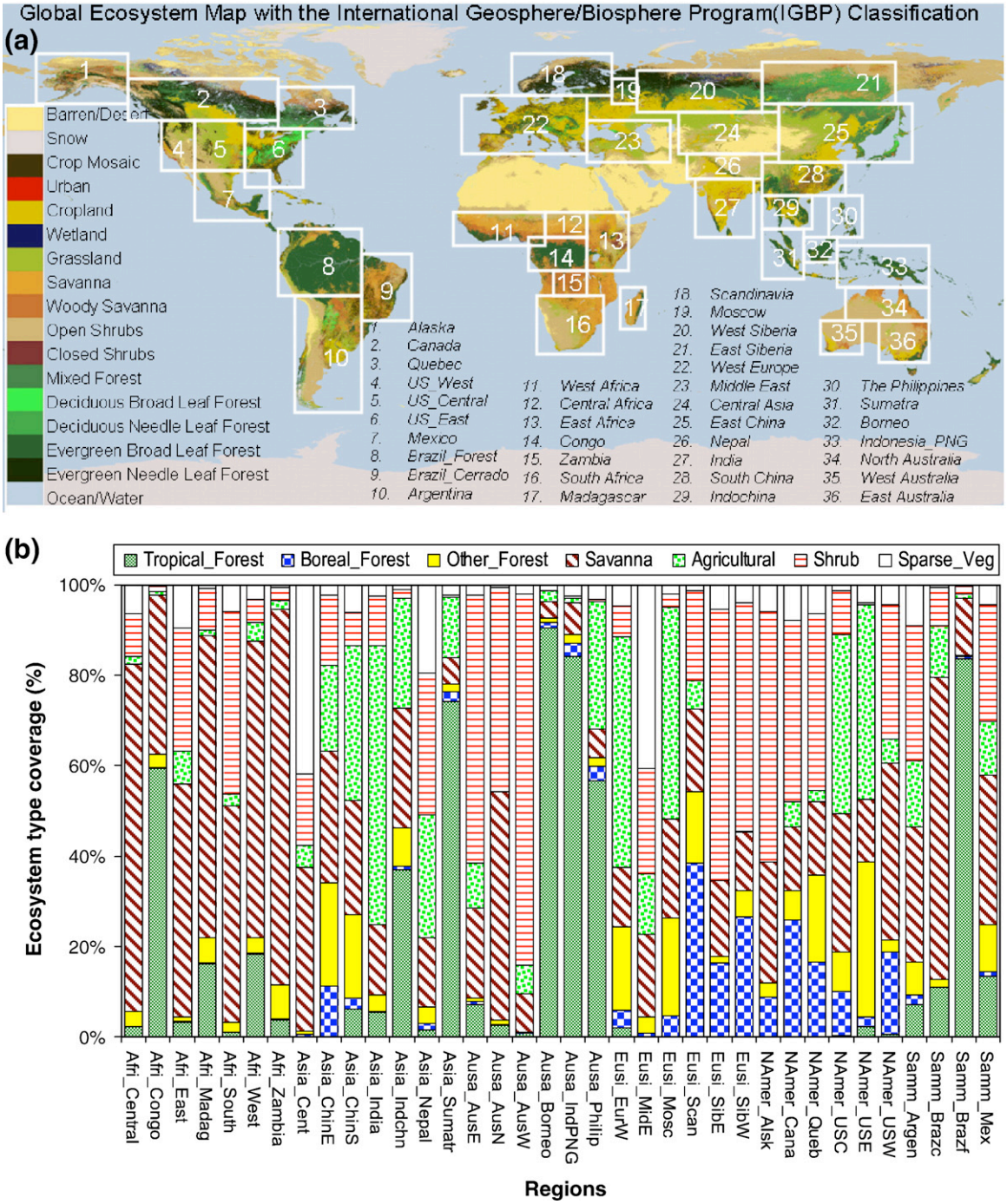

Fig. 3. (a) Global ecosystem map derived from MODIS based on the International Geosphere/Biosphere Program (IGBP) classification scheme. Numbered white boxes delineate different regions identified for independent and comparative analysis in this study, with the names corresponding to the numbers listed. Note that the names are only used for general identification purposes but not to confer political boundaries, (b) proportions of different ecosystem types (grouped into 7 broad classes) relative to the total land surface (as opposed to water) in the area selected for each region.

Table 1
Fire regions selected for this study, as designated by white boxes in Fig. 3, grouped by geographic proximity for convenience in analysis

Map box number	Map box name	Abbreviation	MinLon	MaxLon	MinLat	MaxLat	Total boxed area (km^2)	Land area (km^2)
North America (NAmer)								
1	Alaska	NAmer_Alsk	−170	−140	50	75	4,272,368	1,512,008
2	Canada	NAmer_Cana	−140	−80	50	70	7,420,930	5,376,155
3	Quebec	NAmer_Queb	−80	−55	45	65	3,543,403	1,998,438
4	US_West	NAmer_USW	−130	−105	30	50	4,716,536	3,183,368
5	US_Central	NAmer_USC	−105	−90	25	55	4,217,487	3,746,824
6	US_East	NAmer_USE	−90	−70	25	45	4,030,393	2,107,025
South America and Mexico (Samm)								
7	Mexico	Samm_Mex	−120	−85	10	30	8,068,786	2,301,317
8	Brazil_Forest	Samm_Brazf	−75	−50	−15	5	6,101,279	5,944,056
9	Brazil_Cerrado	Samm_Brazc	−50	−30	−20	0	4,826,646	2,681,500
10	Argentina	Samm_Argen	−75	−45	−60	−20	11,144,894	4,711,171
Africa (Afri)								
11	West Africa	Afri_West	−20	15	0	15	6,390,430	3,774,955
12	Central Africa	Afri_Central	15	30	5	15	1,816,743	1,813,874
13	East Africa	Afri_East	30	50	−10	15	6,101,266	4,233,482
14	Congo	Afri_Congo	10	30	−10	5	3,678,942	3,415,158
15	Zambia	Afri_Zamb	22	35	−18	−8	1,558,250	1,501,480
16	South Africa	Afri_South	10	35	-35	−20	4,094,404	2,544,596
17	Madagascar	Afri_Madag	42	50	−25	−12	1,213,045	577,723
Europe and Siberia (Eusi)								
18	Scandinavia	Eusi_Scan	0	35	55	75	3,662,336	1,573,765
19	Moscow	Eusi_Mosc	30	60	45	60	3,390,692	3,203,115
20	West Siberia	Eusi_Sibw	35	90	60	75	3,919,371	2,604,822
21	East Siberia	Eusi_Sibe	90	140	60	85	4,644,444	2,667,087
22	West Europe	Eusi_Eurw	−10	30	35	55	6,973,738	4,397,184
23	Middle East	Eusi_Mide	30	60	30	45	4,403,681	3,385,794
Asia (Asia)								
24	Central Asia	Asia_Cent	60	110	35	50	6,828,468	6,721,817
25	East China	Asia_Chine	110	150	35	60	8,308,812	5,437,222
26	Nepal	Asia_Nepal	65	95	25	35	3,204,672	3,149,044
27	India	Asia_India	70	90	5	25	4,736,372	2,021,549
28	South China	Asia_Chins	100	125	20	40	5,320,798	3,984,761
29	Indochina	Asia_Indchn	90	110	10	25	3,516,129	2,260,711
Australia and South Asia (Ausa)								
30	The Philippines	Ausa_Philip	115	130	5	20	2,697,972	353,761
31	Sumatra	Ausa_Sumatra	95	110	−10	10	3,674,388	789,014
32	Borneo	Ausa_Borneo	110	120	−5	8	1,596,259	746,023
33	Indonesia_and_PNG	Ausa_Indpng	120	160	−10	5	7,357,883	1,163,820
34	North Australia	Ausa_Ausn	120	150	−20	−10	3,565,581	1,639,540
35	West Australia	Ausa_Ausw	110	130	−35	−20	3,275,523	2,241,252
36	East Australia	Ausa_Ause	135	155	−45	−20	5,169,468	3,027,246

ice-covered regions, which cannot burn. Therefore, the seven ecosystem groups (with their constituents in parenthesis) consist of: Tropical Forest (evergreen broadleaf forest), Boreal Forest (evergreen needleleaf forest, deciduous needleleaf forest), Other Forest (deciduous broadleaf forest, mixed forest), Savanna (woody savanna, savanna, grassland), Agricultural (cropland, crop mosaic), Shrub (closed shrubland, open shrubland), and Sparsely Vegetated (barren/desert, urban and built-up, snow and ice, permanent wetland).

3.2. Regional fire aggregation process

All FRP data, acquired by MODIS on Terra and Aqua from the middle of 2002 to the end of 2006 (4.5 years), were aggregated in such a way as to simplify comparative analysis. Total NFP and mean FRP were calculated for each of the regions at each MODIS local overpass time, which varies between regions even at a given equator crossing time. Local time was calculated using a longitude-dependent time zone information table (http://www.csgnetwork.com/tzitable.html), whereby the local time for areas lying within the 15° longitude range centered on the zero meridian (i.e. from -7.5 ° to 7.5 °) are assumed to be the same as the universal time (UT), beyond which for every additional 15° longitude range toward the East or West, 1 h is added or subtracted, respectively. The median longitude of each region was used to calculate its mean local overpass times, which should only be regarded as approximate, especially for regions that have a very wide longitudinal span.

Although regional mean FRP can act as an indicator of mean subpixel fire intensity and/or size for the relevant overpass time, it does not indicate the total combustion, which can best be represented by the total FRP (i.e. total NFP×mean FRP). However, total NFP or total FRP cannot be compared between regions because of large differences in regional land area and in the overall concentration of fire pixels. To make these quantities comparable between regions, they are here divided by their respective regional land surface areas (in km^2), as listed in Table 1. For total FRP, the result is in units of radiant flux (i.e. MW/km^2 or W/m^2), which can be used to assess the regional fire impact.

3.3. Fire rating scheme based on FRP

The fact that individual pixel FRP values can span three orders of magnitude in range, even within the same locality (Fig. 1b) demonstrates the wide range of possible fire strengths. Therefore, in the case of fire disasters, the FRP values themselves would be too detailed as a means of

communicating the fire status. The strengths of different natural disasters such as hurricanes and earthquakes are expressed in terms of simple dimensionless numerical indices, such as "hurricane category" or "earthquake magnitude", which enable policy makers, disaster managers, and the general public to have a sense of the potential impacts of such events. Large fire disasters potentially have a similarly destructive character as hurricanes and earthquakes. Therefore, it would be useful to devise a similar scale of measurement for describing fire strength. Since MODIS is currently the only sensor capable of measuring the strength of fires (i.e. FRP) globally several times daily, at a (1 km) spatial resolution suitable for characterizing a large proportion of fire events, it is reasonable to establish the fire scale based on the MODIS FRP measures, which will be very informative until a better system can be developed for such categorization.

Since the largest number of fire pixels are observed by MODIS at the Aqua daytime overpass (Fig. 2b), for each fire region considered in this study, these data were binned at 50 MW intervals (0 to <50, 50 to <100, 100 to <150, …) and used to generate histograms, with the frequencies normalized by the maximum frequency for each region and expressed as percentages for comparative plotting (Fig. 4). All regions appear to portray fairly similar frequency distribution shapes, with the smallest bin (0 to <50) having by far the highest frequency, which decreases with higher FRP, although with the exception of a few regions that did not have very high FRP values, several regions showed a second minor mode in the 1500 MW and over range. With limited guidance from these distributions, 5 categories are arbitrarily proposed as a reasonable scale for describing the strength of fires based on the following FRP ranges per pixel: category 1 (<100 MW), category 2 (100 to <500 MW), category 3 (500 to <1000 MW), category 4 (1000 to <1500 MW), and category 5 (≥1500 MW). Note that the first category has the smallest range because most fires fall within this class. Under this scheme, the category of any cluster of fire pixels in any location would be the category of the 1-km resolution pixel with the largest FRP value. Therefore, the 2003 California fires in Fig. 1b would comprise several category 5 fires and a few lower category ones. It is important to note however, that if the fires are observed at a different spatial resolution, then the range of observed FRP values will change, though the total FRP summed over all detected fire pixels in a given area should not (provided all pixels containing actively-burning fires were successfully detected). Fig. 5 shows one example of categories 2 to 5 fires observed by MODIS in the USA, with the attributes, true-color images, and fire category plots in the left, middle, and right columns, respectively. The strengths of the fires are not obvious from the visible images, but are quite vivid on the category plots. It is also possible to use the point system to account for the number of pixels of the highest category in a fire, for better precision, if need be. In that case, the fires in Fig. 5 (top to bottom) may be categorized as: 2.5, 3.3, 4.1, and 5.3, respectively.

One of the potential applications of the fire rating scheme proposed here is that it might be very useful for fire managers who plan crew deployment during major fire events to communicate with the crew, the media, and the general public. If the satellite fire measurement is

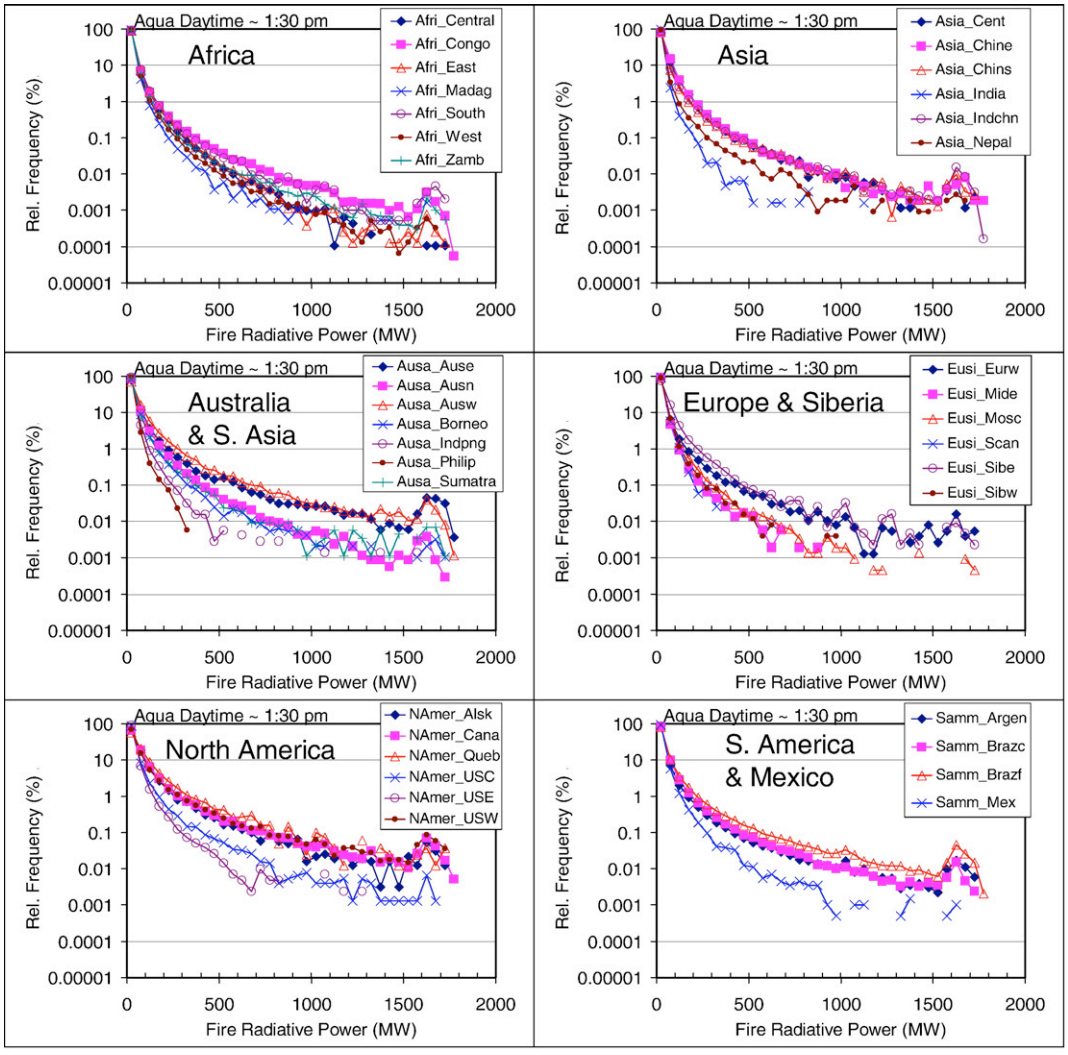

Fig. 4. Regional relative frequency distributions of Fire Radiative Power (FRP) grouped in bins of 50 MW (0 to <50, 50 to <100, 100 to <150, …).

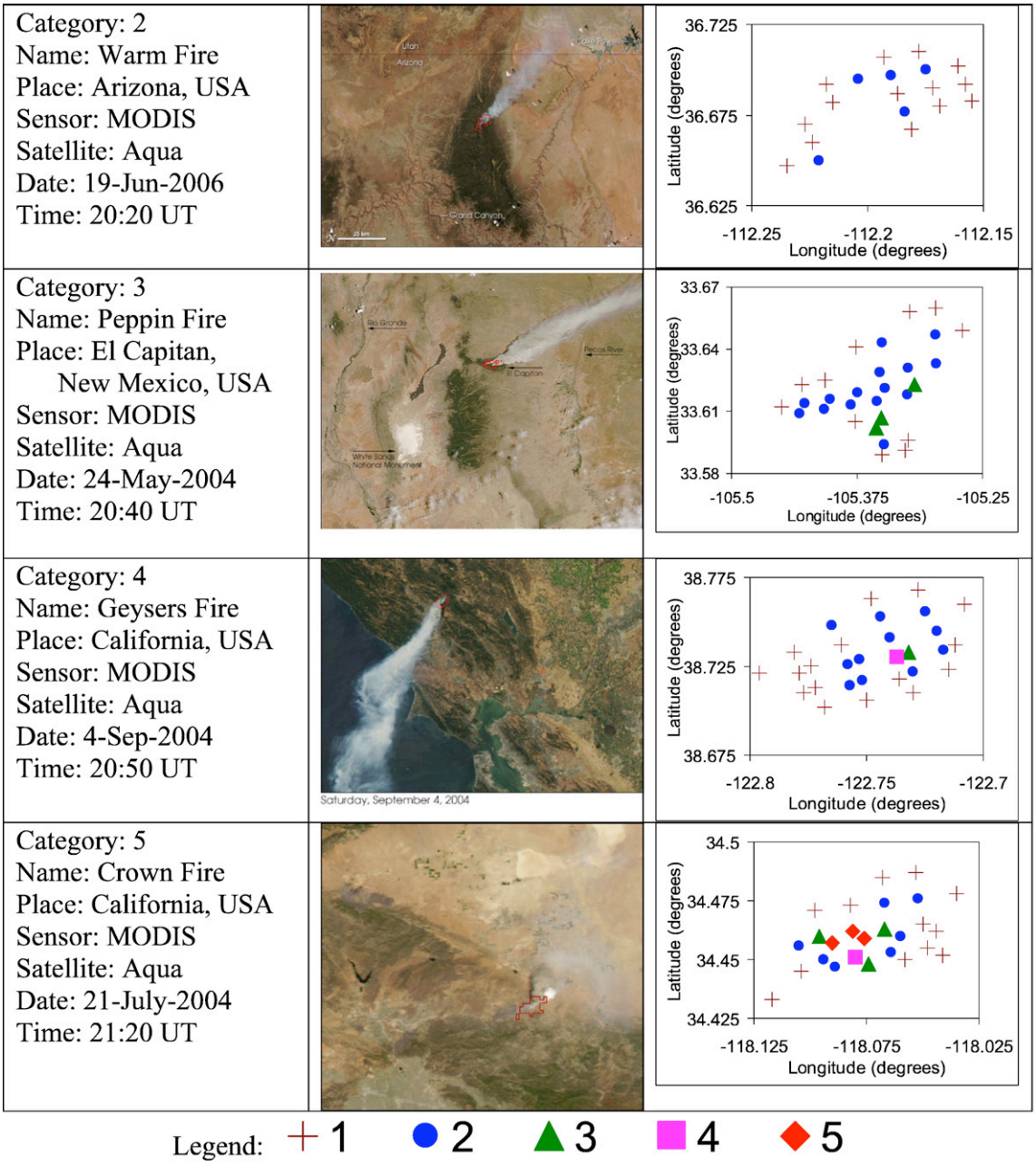

Fig. 5. Examples of fires belonging to categories 2 to 5 (top to bottom rows), with fire attributes (left column), true color MODIS image of fire scenes (middle column), and spatial distribution of pixels of different categories (right column).

acquired in a near real-time fashion, such as from a MODIS Direct Broadcast system (e.g. Huang, 2004), a manager looking at a map of fire category distribution (e.g. Fig. 5) or even a color-coded image of FRP (e.g. Fig. 1b), might use it as an overview planning map to help allocate available fire-suppression equipment and personnel more equitably, in order to achieve an initial optimal deployment of fire suppression resources on a broad scale. The utility of such maps is limited to such broad-scale planning, resource allocation, and follow-up, but not for the actual fire suppression in the field, because of the limited (1-km) spatial resolution of the FRP product.

4. Regional fire regimes and impacts

Although there is no significant diurnal variation in the global mean FRP (Fig. 2a), it is relevant to explore further at regional scales the spatial variability, if any, of the diurnal FRP climatology. Fig. 6 shows plots of mean FRP at the four local MODIS overpass times for each of the 36 fire regions shown in Fig. 3 and Table 1, according to their various geographical groupings. The curves within each panel reflect diversity within each geographical grouping, while the range of vertical scales reflects the differences between the groupings. Assuming homogeneous combustion characteristics for each fire region, differences in mean FRP suggests differences in actual fire sizes within the region. Indeed, in an airborne experiment conducted over a prescribed fire in 1994 in Western USA, Kaufman et al. (1998) found a strong covariance between FRP and fire size. Therefore, for fire regions with little or no FRP diurnal cycle in Fig. 6, it follows that fire size has limited dependence on time of day. The only fire regions that exhibit significant diurnal cycle, with daytime mean FRP being significantly elevated relative to the nighttime values, are the North American boreal-containing (mostly evergreen needleleaf) forests (Alaska, Canada, Quebec, and US_West), as well as East Siberia, and

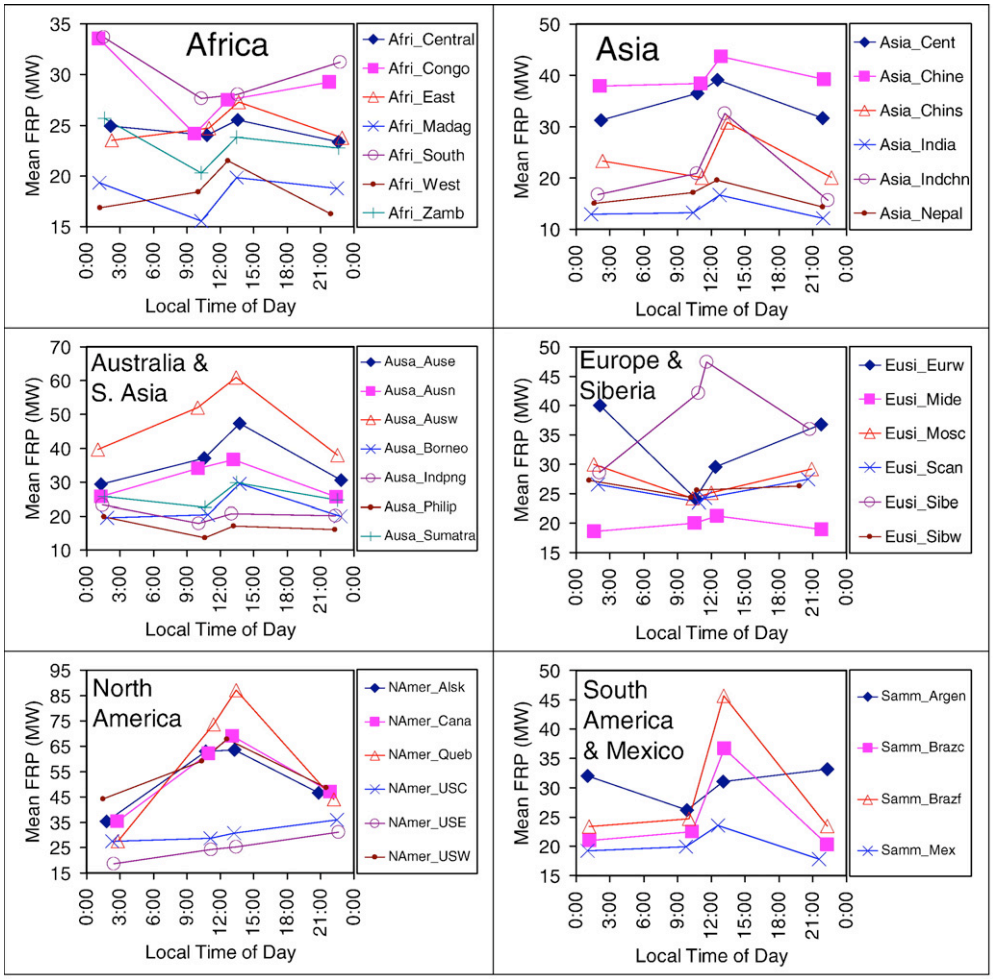

Fig. 6. Regional multi-annual mean Fire Radiative Power (FRP) per nominal 1-km pixel at the four MODIS local mean overpass times.

West, East, and North Australia, in decreasing order of significance. A second group of regions, including the Brazilian (both forest and cerrado) and southern Asian (South China, Indochina, Borneo, and Sumatra) fire regions, maintain approximately the same level of FRP at all overpasses except at the afternoon (Aqua_Daytime) overpass, where they show a peak. Only Western Europe (and to a certain extent also, the Argentina, Congo, South-Africa regions) show a lower mean FRP during the daytime. Discussion of the causes of these regional differences is outside the scope of this study.

The diurnal cycle of fire occurrence can be approximately visualized from plots of mean overpass fire pixel counts (NFP) per 1000-km × 1000-km land area (Fig. 7), which shows that peak fire occurrence is in the afternoon during the Aqua MODIS daytime (AD) overpass for most fire regions, except Alaska (and, to a much lesser extent, East Siberia) whose peak occurs at the late evening Terra MODIS nighttime (TN) overpass. Some regions show more pronounced diurnal variation than others, but in terms of overall magnitude of fire occurrence, the Africa group of regions portrays the highest frequency of fire occurrence per land area, while Europe and North America show the least. Currently, the reason for this discrepancy in the NFP-density diurnal cycle between these groups of fire regions is unclear. However, one obvious inference that can be drawn is that it is not recommended to use fire counts (i.e. NFP) at a single satellite overpass time for estimating burned-biomass or emissions globally, for two main reasons. First, a single daytime overpass cannot truly reflect the relative frequency of fire occurrence between regions, unless the differences in fire diurnal cycle for each region can in some way be established and applied. Second, NFP in different regions cannot be meaningfully compared directly, because there can be significant differences between fire strengths and sizes from one region to another, and also from one time of day to another.

Total FRP, which is the product of the fire counts (NFP) and mean FRP in each fire region, provides a more realistic measure of the regional fire activity, and can be used to quantitatively evaluate fire impact and estimate emissions. The diurnal variation of fire activity between regions can be compared using plots of the mean FRP flux at the four daily overpass times (Fig. 8), which show that most (if not all) of the regions have peak FRP flux at the afternoon (AD) overpass. Based on the vertical scale ranges of the different plots in Fig. 8, the African group of regions shows the highest levels of fire activity, whereas Europe has the lowest.

An idea of the regional seasonal impacts of fires may be obtained from multi-annual (June 2002 to December 2006) monthly mean FRP flux at the peak of the diurnal cycle, which corresponds to the AD overpass (Fig. 9). Although the highest peak monthly mean FRP fluxes in these plots are of the order of 0.05 W/m^2, further analysis revealed that individual overpass values can reach 0.2 W/m^2. These FRP fluxes can be regarded as the active fire contribution to the direct surface radiative forcing (RF) in the different fire regions. These values of fire contribution to regional direct surface forcing are somewhat comparable to those attributed to certain other phenomena in the Intergovernmental Panel on Climate Change (IPCC) Fourth Assessment Report (Forster et al., 2007, pp. 131–132). For instance, black carbon aerosol deposited on snow was estimated to contribute +0.1 ± 0.1 W/m^2 to RF (with a low level of scientific understanding). Detailed discussion of the direct impacts of FRP on radiative forcing is outside the scope of this study, but will likely be the subject of a future paper. The curves in

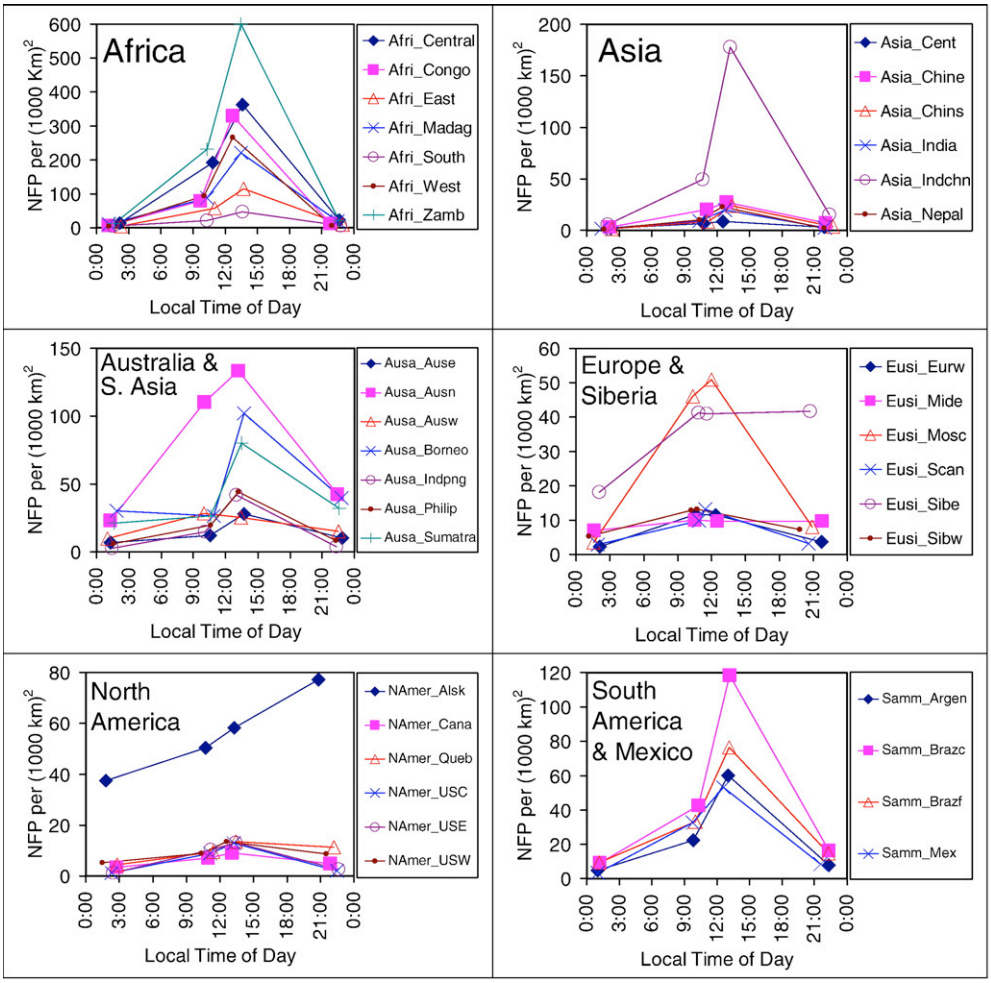

Fig. 7. Regional multi-annual mean fire pixel counts (or number of fire pixels, NFP) per 1000 x 1000-km area at the four MODIS local mean overpass times.

Fig. 9 reflect the relative strengths and seasonal cycles of the fire regimes that characterize the different regions. In Africa, the peak month for the regions north of the Equator (Central and West Africa) is always December, while the peak months for the southern African regions are: Congo in July, Zambia in August, South Africa in September, and Madagascar in October. East Africa has a major peak in December and a minor peak in July, while Congo shows a minor peak in January–February. These results agree with those of a similar analysis based on Terra MODIS fire counts (Giglio et al., 2006a). Other regions of the world also display differences in seasonal cycles, some of which are less distinct than others (Fig. 9).

Since FRP is directly proportional to the rate of biomass consumption (Wooster et al., 2005), assuming that biomass burning is evenly distributed in each of the regions studied, multiplying the FRP flux for any given day and region with the land area of a country within that region will give an estimate of the total FRP released from that country on that day at the AD overpass time. Multiplying that country's overpass total FRP by the value of biomass consumption factor, estimated by (Wooster et al., 2005) as 0.368 kg/MJ, will give the rate of consumption of biomass in that country at that time, which when further multiplied by the representative emission factor for any particulate or gaseous species of biomass-burning emissions, yields the corresponding emission rate of that species.

5. Regional distribution of fire strengths

The FRP-based fire rating scale proposed in this paper can facilitate the analysis of the regional fire strength distribution. Examination of all FRP data acquired at different MODIS overpasses revealed that category 1 fires make up over 90% of fire pixels observed in most regions and overpasses, with a few cases between 80% and 90%, and only Quebec having less than 80% (exactly 77.35%) at the Aqua daytime overpass. The proportion of Category 2 fires is between 0% and 21%, category 3 between 0% and 2%, while each of categories 4 to 5 constitutes less than 0.5% of all fires detected in the different regions; with the Philippines showing no fires above category 2 (Fig. 10). Overall, the proportions of category 1 fires are negatively correlated with those of categories 2 to 5, which are mutually positively correlated with one another (Table 2); showing that regions with tendencies for larger fires have larger proportions of fires in all higher categories (2 to 5), with the highest proportions mostly at the AD overpass time.

A multivariate regression analysis of the proportions of category 2 fires (see Fig. 10) against ecosystem types (see Fig. 3b) was conducted to determine the effect of ecosystem type (if any) on the occurrence of larger fires. The results were inconclusive because there were only 36 data points (fire regions), each of whose ecosystem proportions are a linear combination of one another, thereby preventing unique least squares solutions. However, if Fig. 10 is juxtaposed with Fig. 3b, a visual comparison shows that the North American boreal forests have the highest proportions of large fires. This is in agreement with the aforementioned findings of Wooster & Zhang (2004) and Giglio et al. (2006a). Paradoxically, although the Scandinavian region contains the largest density of boreal forest, it has one of the lowest proportions of categories 2 and 3 fires, and no higher category ones. Similarly, the Brazilian tropical forest has higher proportions of larger fires than the

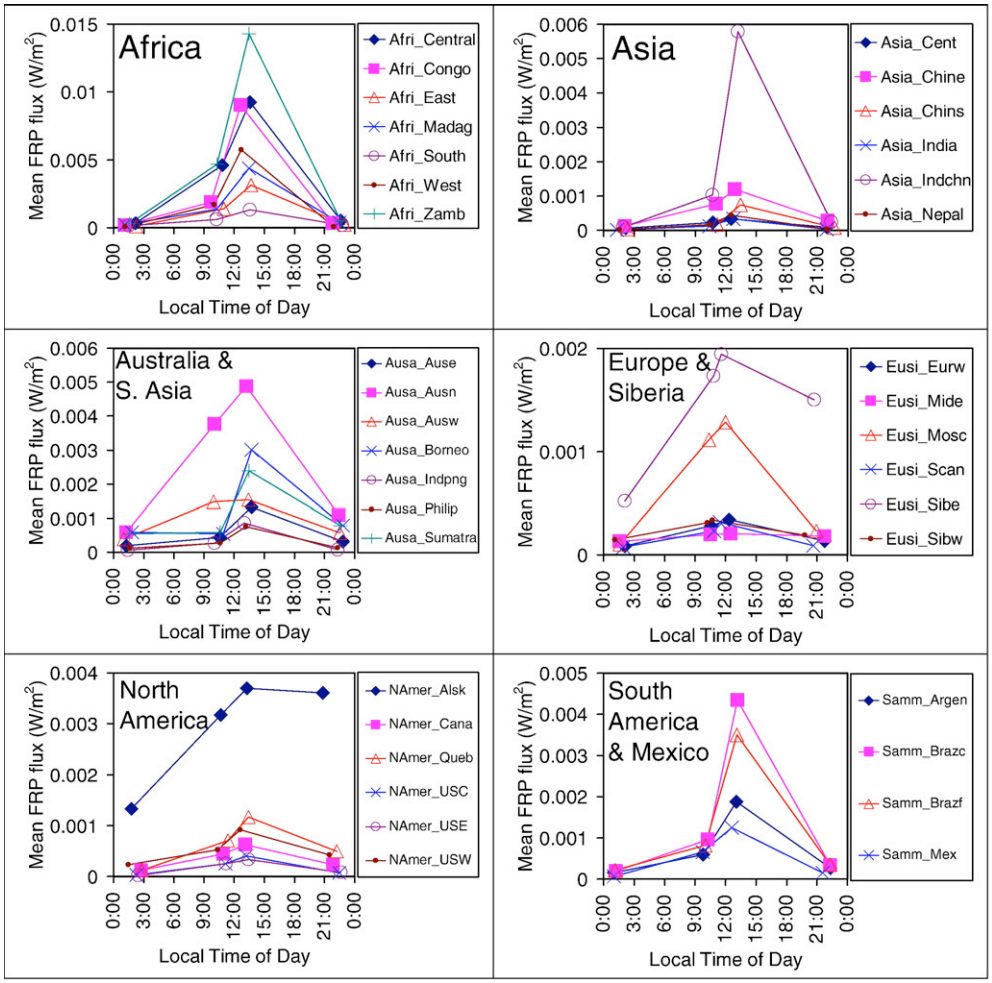

Fig. 8. Regional multi-annual mean Fire Radiative Power (FRP) flux (in W/m^2) at the four MODIS local mean overpass times.

African or Asian regions with comparable density of tropical forest cover. Therefore, ecosystem type alone cannot be used to infer the occurrence of higher category fires, but other factors (probably related to the overall geography and meteorology of the ecosystem specific location, as well as the degree and type of anthropogenic land clearance activities) appear to play a significant role, the determination of which is beyond the scope of this study. However, among the six geographical groupings of fire regions (Table 1), the North American group tends to have the highest proportions of larger fires, while Africa has the lowest. North American boreal forests (Alaska, Canada, Quebec) have a higher frequency of larger fires than those of Eurasia (Scandinavia and West Siberia), which do not have any fires above category 3. Also, although the forest and savanna ecosystems in Brazil are different, in terms of many aspects of their eco-physiological functioning, they do not show large differences in the frequency of larger fires.

One of the major advantages of examining the frequency of occurrence of different fire categories with regard to climate change is that the 2001 report of the Intergovernmental Panel on Climate Change (IPCC) states that "most climate scenarios indicate that the probability of large fires will increase" (IPCC, 2001, sec 13.2.2.1.2). Categorizing fires by strength and assessing their frequency of occurrence will help to establish a baseline upon which future assessments of fire strengths will be based, in order to quantitatively monitor the impact of climate change on fire occurrence.

A preliminary evaluation of the short-term trend of larger fires (categories 2 to 5) has been conducted using Aqua-MODIS daytime (AD) overpass data (which has the greatest significance since it represents the biomass-burning peak time of day for most regions, as Fig. 8 shows). This has been done by analyzing the data according to the six geographical groupings (except that data for the Mexico fire region are included in North America, where it actually belongs), determining the proportions of categories 2 to 5, and plotting their time series (Fig. 11). Obviously, the 5-year period considered is too short to decipher any trend in the frequency of occurrence of these larger fires. Nevertheless, it can still be generalized that North America has the highest peak proportion of larger fires (but only between June and October each year), followed by Australia with the second highest peak proportions (mainly between December and February). Asia, Europe, and South America come third, with fairly comparably highest peaks at categories 2 and 3, although at higher categories (4 and 5) South America maintains third place while Asia and Europe have much lower peak proportions. Overall, Africa always has the lowest peak proportion of larger fires.

6. Discussions and conclusions

This study has provided an assessment of the global and regional patterns of fire activity and strength in a quantitative manner using satellite measurements of fire radiative power (FRP), acquired by the MODIS sensor aboard the Terra and Aqua satellites. It has been shown that fires occur in most vegetated parts of the globe, affecting different types of land-based ecosystems to various degrees. Although FRP values of individual fire pixels measured by MODIS at a nadir 1-km spatial resolution have been found to range from less than 1 MW to over 1800 MW, the global mean FRP at each satellite overpass lies

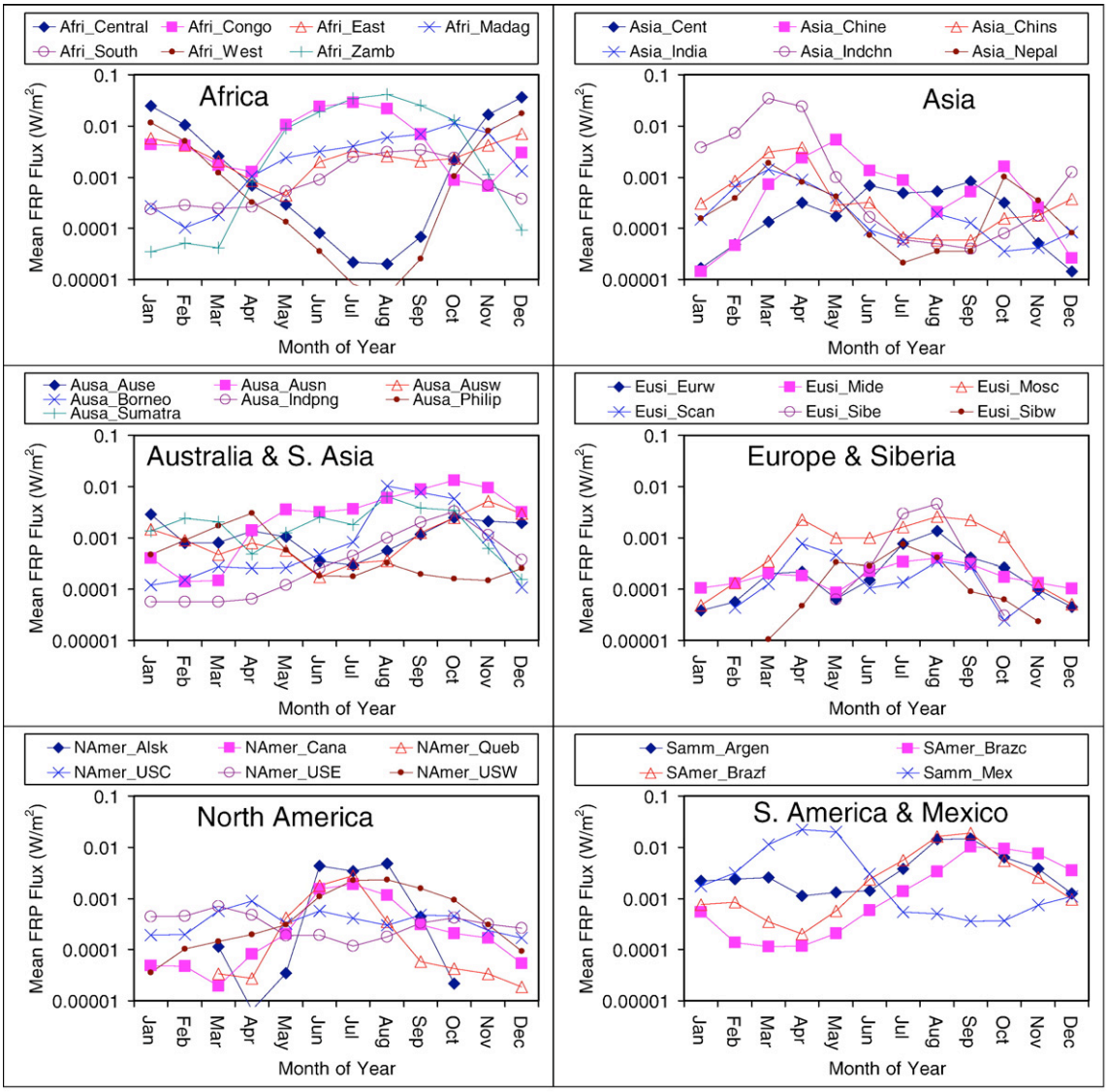

Fig. 9. Multi-year annual cycle of monthly mean FRP flux (in W/m^2) based on MODIS measurements at Aqua daytime (AD) overpass, which occurs at about 1:30 PM across the Equator, and corresponds approximately to the peak biomass-burning time of day in most regions. Note that log scale is used in the vertical axis to accommodate large differences (up to 4 orders of magnitude) between regional peaks and lows.

mostly between 20 and 40 MW per km^2, only falling outside this range in limited cases, but almost never exceeding 80 MW. There is no significant difference in the global mean FRP at the four different local times of day of MODIS overpasses (approximately 1:30 am, 10:30 am, 1:30 pm, and 10:30 pm at the Equator). However, there appears to be a slight seasonal cycle in the global mean FRP, with the minima occurring around March–April, while the maxima are always located in the month of July. On the other hand, the global total number of fire pixels (fire counts) is significantly different between the four times of day, with the minimum count corresponding to the 1:30 am observations, while the maximum count corresponds to the 1:30 pm observations. These minimum and maximum global total fire counts differ by about two orders of magnitude.

An evaluation of the mean FRP by fire region, with differences in dominant ecosystem types, reveals significant differences in the regional diurnal cycles. In most of Africa, mean FRP values at the four overpasses in any given fire region do not differ too much, though they are significantly different between fire regions. Diurnal variation is also subtle in the Moscow area of Russia, the Middle East and Scandinavian fire regions, several parts of Asia, as well as Argentina, Mexico, and Eastern and Central US regions. There is significant diurnal pattern, with prominent peaks at afternoon (1:30 pm) overpasses, in the rest of North America, Eastern Siberia, southern Australia, southern China, Indochina, and the Brazilian fire regions.

Mean FRP fluxes (in W/m^2) in different fire regions shows a diurnal cycle of fire activity with peaks at afternoon (1:30 pm) overpasses in almost all regions, although the peaks are most prominent in the central African regions, Indochina, Northern Australia, Borneo, Sumatra, Moscow, East Siberia, the Brazilian regions, and Alaska. Multi-annual monthly average FRP fluxes at the afternoon (1:30 pm) overpass shows that fires exhibit seasonal cycles in practically all parts of the world, although the peak fire month varies from one fire region to another. For instance, the peak fire month in parts of Africa north of the Equator is around December, while it goes from July to October in various sections of southern Africa. Among all fire regions, the highest peak monthly mean FRP flux is of the order of 0.05 W/m^2, which usually occurs in the peak fire month of every year, although in the low fire season months, it decreases by as much as 3 orders of magnitude, depending on fire region. Indochina and the African fire regions, especially Zambia, Congo, Central and West Africa, portray the highest peak as well as the greatest swing from the high season to the off season periods, whereas other regions have peaks that range from

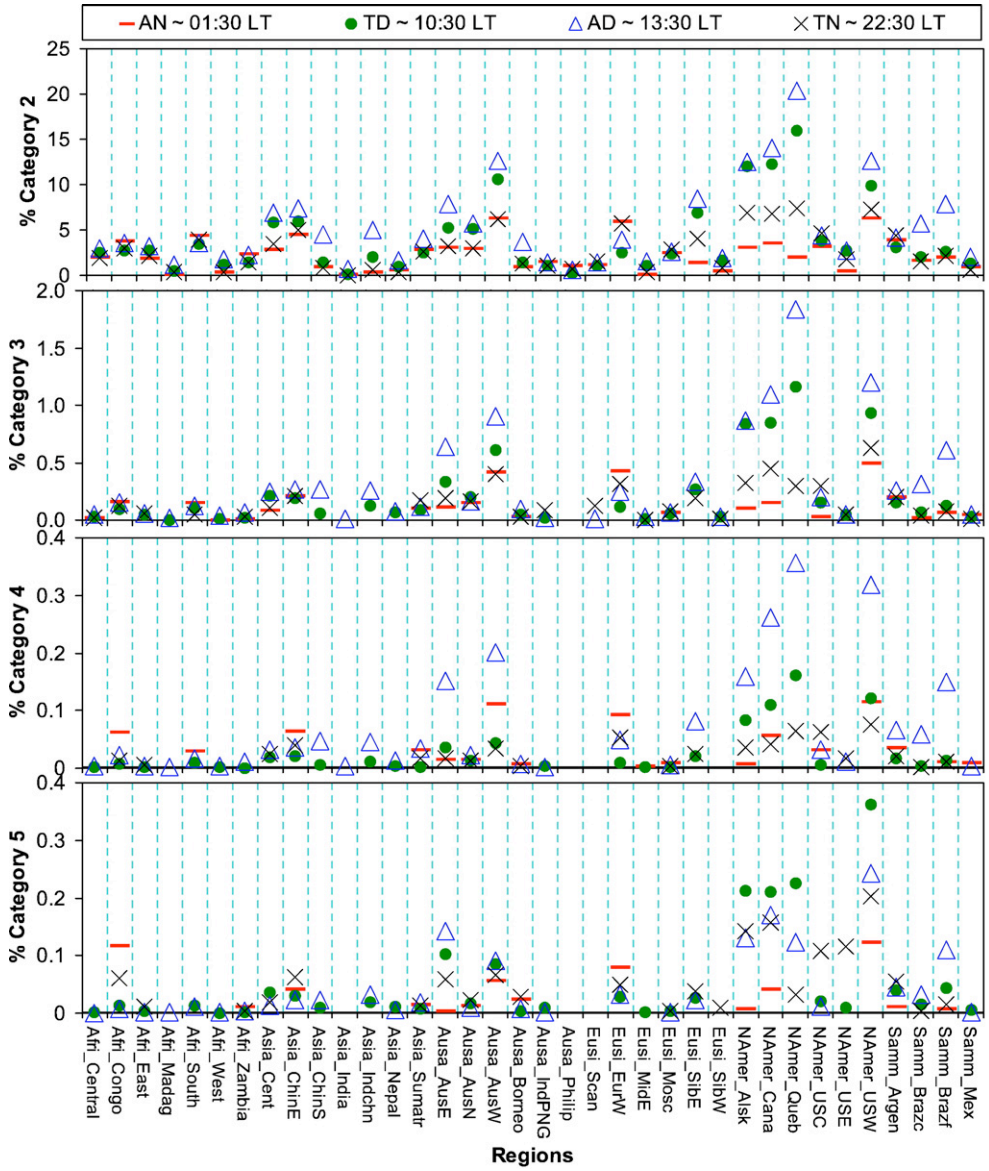

Fig. 10. Regional percent occurrence of categories 2 to 5 fires at four MODIS overpasses (AN = Aqua nighttime, TD = Terra daytime, AD = Aqua daytime, TN = Terra nighttime) derived from all data acquired from June 2002 to December 2006.

less than 50% to less than 1% of the peak values of the above-named regions. In effect, given that FRP is directly proportional to the rate of biomass consumption (Wooster et al., 2005), these FRP flux values reflect the degree of seasonal impact of biomass burning on the ecosystem in various regions, based on current fire regimes.

Categorization of fires based on their FRP values recorded by MODIS has enabled the establishment of a scheme for a simplified fire rating on a scale of 1 to 5, similar to the convention used for other types of disasters (e.g. the Richter scale for earthquakes, the Saffir–Simpson scale for Hurricanes, or the Torino scale for categorizing the impact hazard associated with near-Earth objects (NEOs) such as asteroids and comets). Indeed, remote sensing provides the only practical means of measuring a large range of fire strengths in open-air biomass burning globally, and represents an indispensable tool to monitor fires safely and to provide locational and category information in near real time, for immediate universal understanding of the fire strength, with potential perhaps even to facilitate improved deployment of fire suppression crews and overall management of fires and affected or threatened populations. The fire categorization performed in this study reveals that, with very few exceptions, over 90% of all the fires detected in most regions fall into Category 1, less than 21% in category 2, less than 1% in 3, and less than 0.5% in each of 4 and 5. Ecosystem type alone is not sufficient to explain the frequency of occurrence of the larger fires, which appears to be region-specific, such that at peak fire activity time of day (~1:30 PM) categories 3 to 5 fires are each about an order of magnitude less frequent in the West African savanna than equivalent categories in the Brazilian savanna, whose occurrence frequencies are not too far below those of the Brazilian forest ecosystem. Overall, based on FRP measurements from MODIS from 2002 to 2006 at peak fire times of day represented by the Aqua daytime (AD) overpass, there is no noticeable trend in the frequency of occurrence of larger fires in the MODIS record thus far.

Acknowledgements

We are very grateful to Luke Ellison, who developed the software tool for visualization and analysis of MODIS fire radiative power measurements, as shown in Fig. 1, during his internship at NASA Goddard Space Flight Center in the summer of 2005. We also thank Eric Moody for developing and providing the global land cover map shown and

Table 2
Correlations between the overall proportions of the 5 fire categories from MODIS data for the 36 study regions listed in Table 1

	Cat1%	Cat2%	Cat3%	Cat4%	Cat5%
Aqua nighttime (AN~01:30 LT)					
Cat1%	1.00	−1.00	−0.93	−0.91	−0.69
Cat2%		1.00	0.92	0.89	0.67
Cat3%			1.00	0.93	0.70
Cat4%				1.00	0.79
Cat5%					1.00
Terra daytime (AN~10:30 LT)					
Cat1%	1.00	−1.00	−0.97	−0.93	−0.84
Cat2%		1.00	0.96	0.92	0.83
Cat3%			1.00	0.98	0.93
Cat4%				1.00	0.93
Cat5%					1.00
Aqua daytime (AN~13:30 LT)					
Cat1%	1.00	−1.00	−0.97	−0.95	−0.81
Cat2%		1.00	0.97	0.94	0.80
Cat3%			1.00	0.98	0.86
Cat4%				1.00	0.92
Cat5%					1.00
Terra nighttime (AN~22:30 LT)					
Cat1%	1.00	−1.00	−0.91	−0.87	−0.69
Cat2%		1.00	0.89	0.86	0.66
Cat3%			1.00	0.84	0.79
Cat4%				1.00	0.64
Cat5%					1.00

used for ecosystem analysis in Fig. 3. Many thanks to Mian Chin of NASA/GSFC (USA), Christiane Textor of CEA-Saclay (France), and the four anonymous reviewers for their constructive comments on the pre-publication versions of this paper, as well as Nikisa Jordan for assistance with statistical analysis. Our gratitude also goes to the science and support teams responsible for developing and distributing the MODIS data sets, as well as the NASA Earthobservatory team (http://earthobservatory.nasa.gov/) for providing the beautiful true-color images shown in Figs. 1 and 5. This work was supported by a NASA grant to Charles Ichoku under the atmospheric composition program. The participation of M. J. Wooster in this work was supported primarily by the UK Natural Environment Research Council (NERC) grant NE/C520712/1.

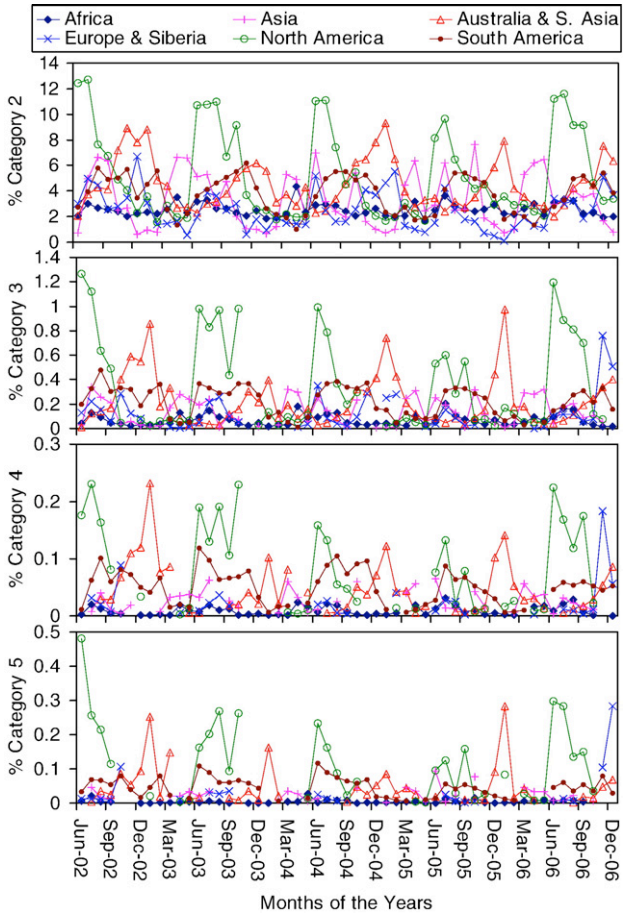

Fig. 11. Time series of monthly mean percent occurrence of categories 2 to 5 fires in large regional groupings, based on MODIS data from the daily Aqua daytime (AD) overpass, which occurs at about 1:30 PM across the Equator, and corresponds approximately to the peak biomass-burning time of day in most regions.

References

Forster, P., Ramaswamy, V., Artaxo, P., Berntsen, T., Betts, R., Fahey, D. W., et al. (2007). Changes in atmospheric constituents and in radiative forcing. In S. Solomon, D. Qin, M. Manning, Z. Chen, M. Marquis, K. B. Averyt, M. Tignor, & H. L. Miller (Eds.), *Climate Change 2007: The Physical Science Basis. Contribution of Working Group I to the Fourth Assessment Report of the Intergovernmental Panel on Climate Change* Cambridge: Cambridge University Press.

Giglio, L., Csiszar, I., & Justice, C. O. (2006). Global distribution and seasonality of active fires as observed with the Terra and Aqua Moderate Resolution Imaging Spectroradiometer (MODIS) sensors. *Journal of Geophysical Research*, *111*, G02016. doi: 10.1029/2005JG000142.

Giglio, L., Descloitres, J., Justice, C. O., & Kaufman, Y. J. (2003). An enhanced contextual fire detection algorithm for MODIS. *Remote Sensing of Environment*, *87*, 273–282.

Giglio, L., Kendall, J. D., & Justice, C. O. (1999). Evaluation of global fire detection algorithms using simulated AVHRR infrared data. *International Journal of Remote Sensing*, *20*(10), 1947–1985. doi:10.1080/014311699212290.

Giglio, L., van der Werf, G. R., Randerson, J. T., Collatz, G. J., & Kasibhatla, P. S. (2006). Global estimation of burned area using MODIS active fire observations.*Atmospheric Chemistry and Physics*, *6*, 957–974. SRef-ID: 1680-7324/acp/2006-6-957.

Huang, H. L., Gumley, L. E., Strabala, K., Li, J., Weisz, E., Rink, T., Baggett, et al. (2004). International MODIS and AIRS Processing Package (IMAPP): a direct broadcast software package for the NASA earth observing system. *Bulletin of the American Meteorological Society*, *85*, 159–161.

Ichoku, C., & Kaufman, Y. J. (2005). A method to derive smoke emission rates from MODIS fire radiative energy measurements. *IEEE Transactions on Geoscience and Remote Sensing*, *43*(11), 2636–2649.

IPCC (Intergovernmental Panel on Climate Change), 2001. in Third Assessment Report (TAR), Climate Change 2001, The Scientific Basis, Contribution of Working Group I to the Third Assessment Report of the International Panel on Climate Change, edited by J. T. Houghton et al., 801 pp., Cambridge Univ. Press, New York, 2001.

Kaufman, Y. J., Justice, C. O., Flynn, L. P., Kendall, J. D., Prins, E. M., Giglio, L., et al. (1998). Potential global fire monitoring from EOS-MODIS. *Journal of Geophysical Research*, *103*, 32215–32238.

Kelhä, V., Rauste, Y., Häme, T., Sephton, T., Buongiorno, A., Frauenberger, O., et al. (2003). Combining AVHRR and ATSR satellite sensor data for operational boreal forest fire detection. *International Journal of Remote Sensing*, *24:8*, 1691–1708. doi:10.1080/01431160210144705.

Roberts, G., Wooster, M. J., Perry, G. L. W., Drake, N., Rebelo, L. -M., & Dipotso, F. (2005). Retrieval of biomass combustion rates and totals from fire radiative power observations: Application to southern Africa using geostationary SEVIRI imagery. *International Journal of Remote Sensing*, *110*, D21111. doi:10.1029/2005JD006018.

Robinson, A. H., & Sale, R. D. (1969). *Elements of cartography*, (3rd edition) New York: John Wiley & Sons, Inc.

Salomonson, V. V., Barnes, W. L., Maymon, P. W., Montgomery, H. E., & Ostrow, H. (1989). MODIS: advanced facility instrument for studies of the earth as a system. *IEEE Transactions on Geoscience and Remote Sensing*, *27*(2), 145–153.

Tansey, K., Grégoire, J. -M., Stroppiana, D., Sousa, A., Silva, J., Pereira, J. M. C., et al. (2004). Vegetation burning in the year 2000: global burned area estimates from SPOT VEGETATION data. *Journal of Geophysical Research*, *vol. 109*, D14S03. doi:10.1029/2003JD003598.

Wooster, M. J. (2002). Small-scale experimental testing of fire radiative energy for quantifying mass combusted in natural vegetation fires. *Geophysical Research Letters*, *29*(21), 2027. doi:10.1029/2002GL015487.

Wooster, M. J., Roberts, G., Perry, G. L. W., & Kaufman, Y. J. (2005). Retrieval of biomass combustion rates and totals from fire radiative power observations: FRP derivation and calibration relationships between biomass consumption and fire radiative energy release. *Journal of Geophysical Research*, *110*, D24311. doi:10.1029/2005JD006318.

Wooster, M. J., & Zhang, Y. H. (2004). Boreal forest fires burn less intensely in Russia than in North America. *Geophysical Research Letters*, *vol. 31*, L20505. doi:10.1029/2004GL020805.

Wooster, M. J., Zhukov, B., & Oertel, D. (2003). Fire radiative energy for quantitative study of biomass burning: derivation from the BIRD experimental satellite and comparison to MODIS fire products. *Remote Sensing Environment*, *86*, 83–107.